Experimental Cell Research 445 (2025) 114408

Contents lists available at ScienceDirect

Experimental Cell Research

journal homepage: www.elsevier.com/locate/yexcr

Research article

Matrix-mediated activation of murine fibroblast-like synoviocytes

Isabel Zeinert [a,*], Luisa Schmidt [b], Till Baar [c], Giulio Gatto [d], Anna De Giuseppe [e], Adelheid Korb-Pap [e], Thomas Pap [e], Esther Mahabir [f], Frank Zaucke [d], Bent Brachvogel [g,h], Marcus Krüger [b,i], Thomas Krieg [a,i,j], Beate Eckes [a,**]

[a] Translational Matrix Biology, University of Cologne, Medical Faculty, Cologne, Germany
[b] Institute for Genetics, Cologne Excellence Cluster on Cellular Stress Responses in Ageing-Associated Diseases (CECAD), University of Cologne, Cologne, Germany
[c] Institute for Medical Statistics and Computational Biology, Faculty of Medicine, University of Cologne, Cologne, Germany
[d] Rolf M. Schwiete Research Unit for Osteoarthritis, Department of Trauma Surgery and Orthopedics, Goethe University Frankfurt, University Hospital, Frankfurt am Main, Germany
[e] Institute of Musculoskeletal Medicine, University Hospital Muenster, Muenster, Germany
[f] Comparative Medicine, Center for Molecular Medicine Cologne (CMMC), University of Cologne, Faculty of Medicine and University Hospital Cologne, Cologne, Germany
[g] Center for Biochemistry, University of Cologne, Faculty of Medicine, Cologne, Germany
[h] Department of Pediatrics and Adolescent Medicine, Faculty of Medicine and University Hospital Cologne, University of Cologne, Cologne, Germany
[i] Center for Molecular Medicine (CMMC), University of Cologne, Cologne, Germany
[j] Cologne Excellence Cluster on Cellular Stress Responses in Ageing-Associated Diseases (CECAD), University of Cologne, Cologne, Germany

ARTICLE INFO

Keywords:
Extracellular matrix
Chondrocytes
Rheumatoid arthritis
Cytokines

ABSTRACT

Fibroblast-like synoviocytes (FLS) are key cells promoting cartilage damage and bone loss in rheumatoid arthritis (RA). They are activated to assume an invasive and migratory phenotype. While mechanisms of FLS activation are unknown, evidence suggests that pre-damaged extracellular matrix (ECM) of the cartilage can trigger FLS activation. Integrin α11β1 might be involved in the activation, as it is increased in RA patients and hTNFtg mice, an RA mouse model.

We treated murine chondrocytes with TNFα to produce a damaged, RA-like matrix. Comparison to healthy chondrocyte matrix revealed decreased ECM proteins, e.g. collagens and proteoglycans, increased matrix-degrading proteins and elevated levels of inflammatory cytokines.

FLS responded to the damaged chondrocyte matrix with a matrix-remodeling and pro-inflammatory phenotype characterized by a gene signature involved in matrix degradation and increased production of CLL11 and CCL19. Damaged chondrocyte matrix stimulated increased *Itga11* expression in FLS, correlating with the increased α11β1 amounts in RA patients. FLS deficient in integrin α11β1 released lower amounts of inflammation-associated cytokines.

Our results demonstrate differences in healthy and RA-like chondrocyte ECM and distinctly different responses of wt FLS to damaged versus healthy ECM.

Abbreviations: ADAM, A disintegrin and metalloproteases; ADAMTS, ADAMs with thrombospondin motifs; C&M, Cells & deposited matrix; CCL, C-C motif chemokine; CILP, Cartilage intermediate layer protein; COL, Collagen; COMP, Cartilage oligomeric matrix protein; CXCL, C-X-C motif chemokine; DEG, Differentially expressed genes; ECM, Extracellular matrix; FLS, Fibroblast-like synoviocytes; GSEA, Gene set enrichment analysis; Itga, Integrin alpha; KEGG, Kyoto encyclopedia of genes and genomes; LC-MS/MS, Liquid chromatography–mass spectrometry; Log2FC, Log2 fold change; MMP, Matrix metalloproteinase; NES, Normalized enrichment score; RA, Rheumatoid arthritis; TGFβ, Transforming growth factor beta; TNFα, Tumor necrosis factor alpha; UMAP, Uniform Manifold Approximation and Projection; wt, Wild type.

* Corresponding author. Translational Matrix Biology University of Cologne, Faculty of Medicine Joseph-Stelzmann-Str. 52 (Buildg. 44) 50931, Cologne, Germany.
** Corresponding author.
E-mail addresses: isabel.zeinert@uk-koeln.de (I. Zeinert), beate.eckes@uni-koeln.de (B. Eckes).

https://doi.org/10.1016/j.yexcr.2025.114408
Received 21 June 2024; Received in revised form 14 December 2024; Accepted 3 January 2025
Available online 5 January 2025

1. Introduction

One of the most prevalent joint diseases is rheumatoid arthritis (RA), a chronic inflammatory autoimmune disease that mainly affects synovial joints. Disease progression is characterized by chronic systemic inflammation, as well as destruction of different tissues in the joint including bone and cartilage that can cause lifelong disabilities [1].

The destruction of the joint is mediated by several synergizing factors. Invading T and B cells secrete inflammatory cytokines leading to activation of FLS in the synovial membrane. Those activated FLS show increased proliferation due to cytokine stimulation and decreased apoptosis associated with changes in the mitochondrial pathway [2,3]. Hence, the synovial lining that comprises only a few cell layers in healthy conditions, transforms into a pannus, which is an invasive hyperplastic tissue mass. The activated FLS show an aggressive and invasive phenotype and contribute to the progressive destruction of cartilage and bone by expression of cytokines, chemokines, pro-angiogenic factors and MMPs, which leads to sustained inflammation, increased angiogenesis and ECM destruction, respectively [4]. Similar invasiveness is known to characterize tumor cells that use invadopodia, actin-rich structures, for proteolytic attack on the surrounding ECM [5]. Cartilage degradation in arthritis has been associated with similar structures [6].

Implantation of RA-FLS into the knee joint of immunocompromised mice induce development of arthritis in that joint, while FLS from healthy donors do not cause arthritis [7]. Moreover, the implanted RA-FLS are capable of migrating to distant healthy cartilage, as shown by implantation of a sponge-cartilage complex containing RA-FLS into immunocompromised mice. The RA-FLS detached from the site of implantation and migrated through the blood stream to a further distant implanted sponge-cartilage complex that they invaded. Those results indicated a crucial role for immune cell-independent pathways in RA and raised the question if cartilage ECM may have a role in activating FLS and transforming them into invasive cells [8]. This is in line with the observation that cartilage destruction in hTNFtg mice, a well-characterized mouse model that develops chronic inflammatory arthritis [9], precedes the attachment of the synovial membrane to the cartilage. This suggests that the damaged cartilage acts as a stimulus for FLS attachment and invasion [10].

The mechanisms of FLS activation by damaged cartilage are currently not understood. There is increasing evidence suggesting, that ECM fragments are released during cartilage destruction that subsequently act as ligands for cell surface receptors on FLS [8]. Hence, besides inflammatory factors that induce FLS activation, cartilage itself may not only be the target of invasive FLS, but may also trigger FLS activation [11]. Thereby the interaction between ECM and FLS is crucial. Several lines of evidence suggested that collagen-binding integrin α11β1 [12] could be an important receptor in this interaction: α11β1 expression is strongly elevated in the synovium of RA patients as well as in diseased hTNFtg mice compared to healthy donors and WT mice, while ablation of α11β1 in hTNFtg mice leads to a milder disease progression, less cartilage and bone damage and reduced FLS attachment, indicating a crucial role of α11β1 in RA [1,13]. Elevated α11β1 expression has previously been associated with activation of skin fibroblasts in wound repair and dermal fibrosis [14], seen in cancer-associated fibroblasts of several tumor tissues [12,15], and shown to impact MMP synthesis [16].

Here, we investigated the differential influence of a chondrocyte matrix deposited either by healthy or RA-like chondrocytes on FLS activation and compared the response of FLS lacking integrin α11β1 to wt FLS.

2. Results

2.1. Generation of healthy and RA-like chondrocyte extracellular matrices

To produce sufficient amounts of chondrocyte matrix for analysis at the transcript and protein levels, primary murine chondrocytes were isolated from tibial and femoral epiphyses and cultured at high density for 14 days (Fig. 1). TGFβ3 was added as indicated in Fig. 1A to stimulate the differentiation into an articular chondrocyte phenotype [17], demonstrated by induced *Prg4* [18] and *Cilp2* transcripts [19,20] and stable expression of collagen II and aggrecan (Fig. 1B–D). To induce an RA-like (damaged) matrix, cultures were treated with TNFα for 10 days (Fig. 1E–G). These treatment conditions gave rise to decreased gene expression and reduced protein abundance of aggrecan, collagen II and COMP in TNFα-treated cultures (Fig. 1E and F) as well as to visible loss of matrix, in particular of proteoglycan matrix, as shown by Alcian blue staining, while abundant matrix was accumulated by untreated (ctrl) chondrocyte cultures, and a change in distribution from a clumpy towards a rather homogeneous matrix staining (Fig. 1G). These cultures were thus suited to analyze the extracellular matrices deposited by healthy or RA-like chondrocytes by subsequent transcript and proteome analysis. After 14 days of culture, FLS were seeded on top of these matrices to characterize their response to damaged versus healthy chondrocyte ECM. In order to decipher the FLS response to the chondrocyte ECM, the cultures were subjected to three cycles of freeze/thaw and extensive washing, which efficiently removed chondrocyte cellular debris (not shown). Following this decellularization step, the matrices were used for seeding with synovial fibroblasts for 72 h as indicated in Fig. 1A.

2.2. Transcriptional response of chondrocytes to TNFα

Bulk transcriptomes of TNFα-treated versus untreated (ctrl) chondrocytes were compared by RNA sequencing (RNA-seq). In total, 17,368 transcripts were identified, of which 2139 were differentially expressed genes (DEG; $|\text{fold change}| > 1.5$ and adjusted p-value <0.05). Of these, 1378 genes were significantly upregulated and 761 genes were significantly downregulated by TNFα treatment of chondrocytes. Hierarchical clustering based on the most frequently identified transcripts (base mean $>$ 28,000) revealed upregulation of transcripts encoding matrix degrading proteins (*Mmp3* and *Mmp13*) and chemokines (*Ccl2*, *Ccl5*, *Cxcl12*) (Fig. 2A). In contrast, expression of several ECM proteins, including cartilage markers (*Col2a1, Col9a1, Col11a1 and a2, Comp*, *Acan*), was downregulated. Gene Set Enrichment Analysis (GSEA) for KEGG (Kyoto Encyclopedia of Genes and Genomes) pathways confirmed activated 'TNF'- and 'chemokine signaling pathway' and revealed suppressed 'ECM-receptor interaction' within the top 4 upregulated and all 4 downregulated pathways ranked by normalized enrichment score (NES) (Fig. 2B). RT-PCR analysis confirmed the RNA-seq data for selected transcripts (Fig. 2C).

2.3. Differences in soluble cytokine levels produced by untreated and TNFα-treated chondrocytes

Since transcript levels do not always reflect the actual protein levels due to posttranscriptional regulation, and given the relevance of chemokines and cytokines in RA [21], we determined their levels in ctrl and TNFα-treated chondrocytes directly using bead-based assays. We concentrated on soluble mediators released to culture supernatants, since it is difficult to detect cytokines and inflammatory mediators in total protein samples by mass spectrometry due to their low abundance. This implies that we may miss some of those cytokines that are bound to matrix proteins. Overall, TNFα treatment resulted in increased release of several cytokines and chemokines in comparison to untreated cultures, and significantly increased levels of CCL5, CXCL2, CXCL16, CX3CL1, LIF

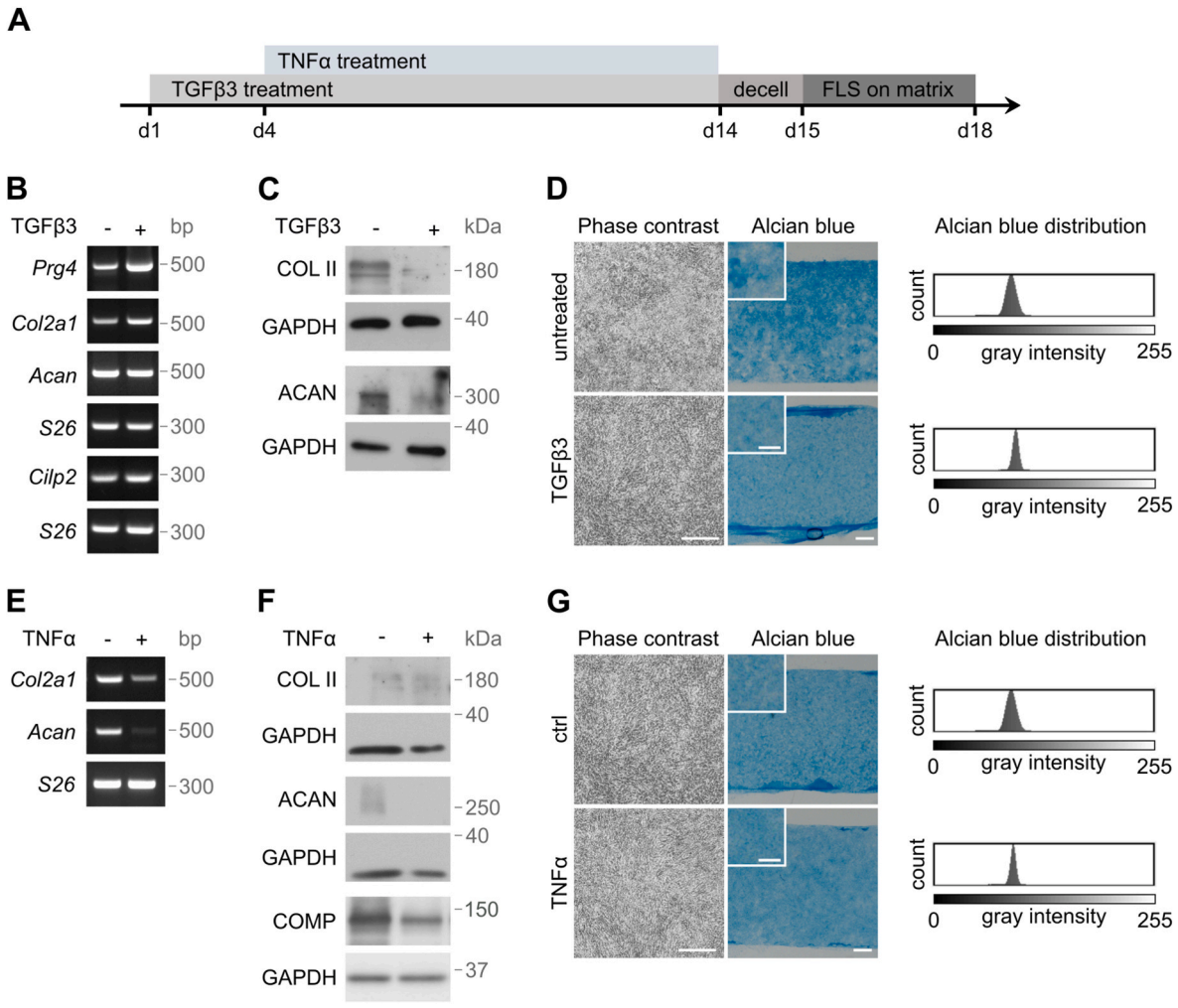

Fig. 1. Characteristics of the culture model used to generate healthy and RA-like chondrocytes matrices. A. Chondrocytes isolated from tibial and femoral epiphyses were seeded at high density (50,000 cells per culture insert) to generate ECM. TGFβ3 was added (10 ng/ml) to all cultures and TNFα was supplied (100 ng/ml) as indicated only to cultures depositing the damaged matrix. Matrices were decellularized and either analyzed directly or decellularized and seeded with FLS for 72 h. **B-D.** Alcian blue staining showing that TGFβ3 treatment alone did not alter deposited proteoglycan material (**B**) nor collagen II or aggrecan transcript levels, while it induced an articular cartilage-like phenotype indicated by enhanced expression of *Prg4* and *Cilp2* (**C**) but lead to some reduction in protein levels and a clear change in color distribution towards a homogeneous matrix. n = 4 (**D**). **E-G.** Damaged chondrocyte matrix generated by treatment of cultures with TNFα, analyzed at d14 before decellularization, showed reduced levels of collagen II and aggrecan transcripts (**E**) and reduced aggrecan, collagen II and COMP protein levels (**F**), as well as reduced amounts of proteoglycan ECM illustrated by Alcian blue staining (**G**). The narrow peak in the histogram indicates a shift towards a homogeneous distribution of Alcian blue positive matrix in comparison to the wide peak in untreated cultures. Scale bars in D and G represent 200 μm in phase contrast images, 500 μm in Alcian blue images and 200 μm in magnified insets.

and M-CSF were detected (Fig. 3A). Levels of IL6, CCL20, CCL2 and CCL24 tended to be higher upon TNFα treatment, while secretion of CXCL1 and CXCL5 remained unchanged (Fig. 3B), and levels of VEGF, CCL7 and CXCL12 were in part significantly reduced (Fig. 3C). Furthermore, GM-CSF, FGF2, CXCL9, CCL3 and CCL12 were detected only at low concentrations in the supernatants.

2.4. *Proteome analysis of healthy and damaged ECM deposited by chondrocytes*

We then concentrated on the analysis of decellularized matrices deposited by TNFα-treated or ctrl (untreated) chondrocytes. The proteome of deposited matrix plus chondrocytes was also assessed by mass spectrometry (cells plus deposited matrix, termed C&M in Fig. 4) in order to confirm the efficient removal of cellular proteins by decellularization. The mean intensity of decellularized matrix (decell) produced by untreated chondrocytes (ctrl) was plotted against the cellular proteins together with those in the deposited matrix (C&M). Results indicated lower intensities for the majority of actin cytoskeleton proteins (GO:0015629; shown as dark grey dots) in the decell fraction, while the intensities for the majority of ECM proteins in ctrl decell were increased (GO:0031012; shown as red dots) (Fig. 4A). This demonstrated that decellularization had successfully depleted most intracellular proteins, e.g. cytoskeleton components, and as a consequence, ECM proteins were strongly enriched in the decell fraction. The differences in the matrices deposited by TNFα-treated versus untreated (ctrl) chondrocytes are shown in Fig. 4B–D. Comparison of these proteomes revealed 751 differentially abundant proteins upon TNFα treatment, of which 42 belong to the core matrisome and 35 to the matrisome-associated group of ECM proteins [22] (Fig. 4B). The volcano plot (Fig. 4C and Suppl. Table 1) depicts many of these core matrisome and matrisome-associated proteins that are significantly regulated in the TNFα-treated decellularized chondrocyte matrix (marked by dark red dots). Many different collagens (COL1A1, COL1A2, COL2A1, COL5A1, COL5A2, COL12A1, COL14A1), but also aggrecan and chondroadherin were strongly downregulated in the damaged matrix, while

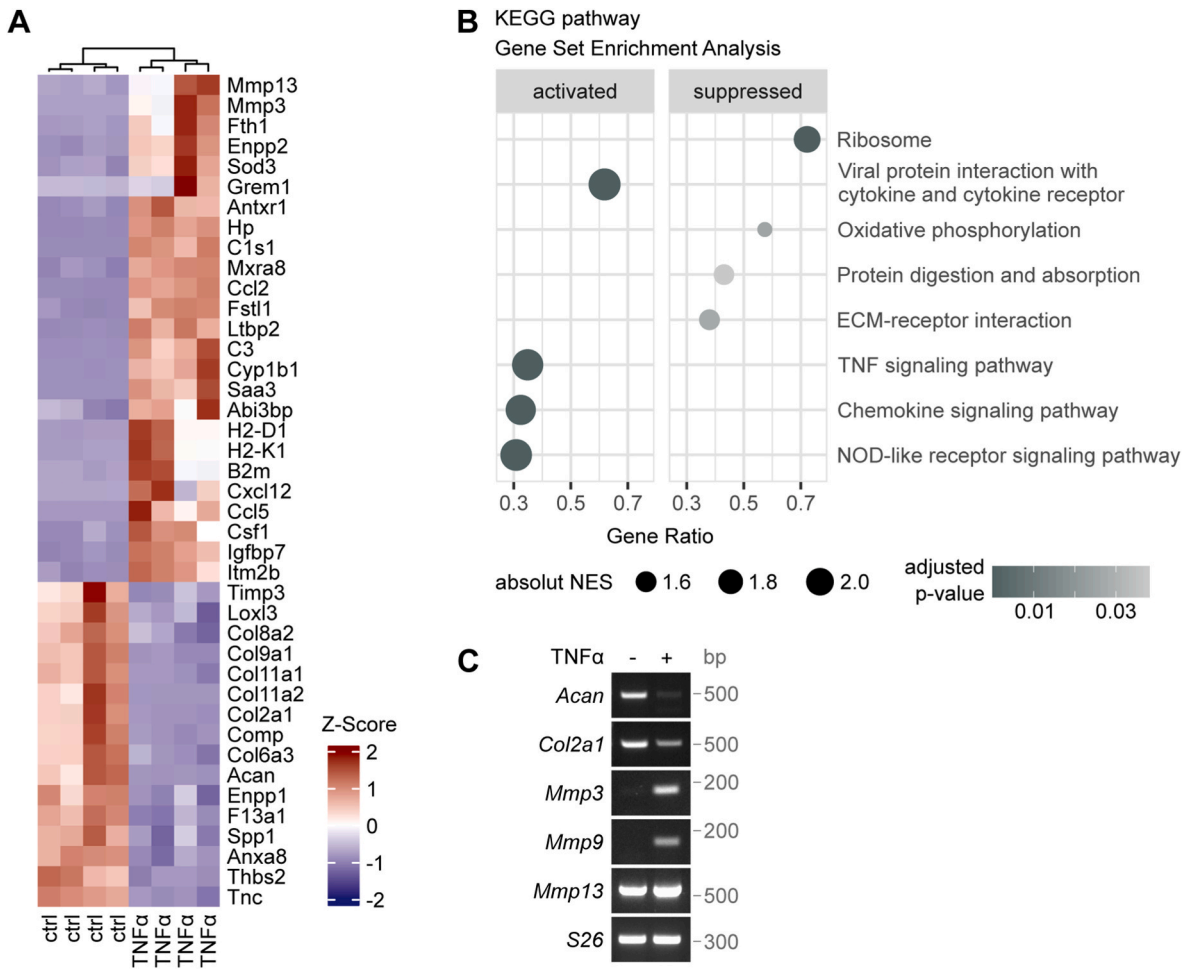

Fig. 2. Transcriptional changes in TNFα-treated versus ctrl chondrocytes. Cultures were treated as shown in Fig. 1A and subjected to RNA-seq analysis at d14 prior to decellularization. **A.** Hierarchical clustering showing the z-transformed expression values of the most frequently identified transcripts (base mean > 28,000). **B.** Gene Set Enrichment Analysis for KEGG pathways showing the top 4 activated and all 4 suppressed pathways ranked by normalized enrichment score (NES). n = 4. **C.** RT-PCR of selected chondrocyte transcripts detected in (A) expressed by TNFα-treated and ctrl chondrocytes.

matrix-degrading enzymes including MMP2, -3, -13 and −19 and ADAMTS5 and ADAMTSL4 were upregulated.

Screening for proteins that were solely detected in one condition (either untreated ctrl or TNFα-treated decellularized matrix) and not in the other revealed a considerable number of proteins for each condition, illustrated by dark grey and dark blue dots in Fig. 4D. Of note, proteins only deposited in the ECM by TNFα-treated chondrocytes included MMP9, -10 and −12 and inflammation-related cytokines CCL5 and CCL20. The mean intensities of those proteins were higher than the median of all measured intensities, and imputed data confirmed significant upregulation of these proteins (Suppl. Table 2).

2.5. Transcriptional responses induced in FLS by chondrocyte matrices

To investigate the influence of a chondrocyte-generated ECM on FLS phenotype, FLS were seeded on either healthy (undamaged) or RA-like (damaged, deposited by TNFα-treated chondrocytes) decellularized chondrocyte matrices. In addition, FLS isolated from $\alpha11^{-/-}$ mice were cultured on these matrices to define the importance of this receptor that is elevated in FLS of RA patients and in mouse models of RA [1] for the response to the ECM. Both, wt and $\alpha11^{-/-}$ FLS were capable of adhering to and spreading on undamaged and damaged chondrocyte matrices (Fig. 5A). Differential responses of wt and $\alpha11^{-/-}$ FLS to the two matrix types were determined by bulk RNA-seq analysis. UMAP based on 17, 148 identified transcripts did not reveal a clear separation between the clusters of wt and $\alpha11^{-/-}$ FLS seeded on damaged or healthy chondrocyte matrices (Fig. 5B). However, a tendency was discernible, revealing a separation according to undamaged or damaged matrix (indicated by light and darker grey shading). The ratio of transcriptional changes in wt FLS on damaged versus undamaged matrix was plotted against the ratio of transcriptional changes in $\alpha11^{-/-}$ FLS on damaged versus undamaged matrix (Fig. 5C). This scatter plot also revealed that there were no major differences in the response of wt versus $\alpha11^{-/-}$ FLS to the damaged chondrocyte matrix. Some candidates are depicted by name because they were detected at considerable abundance (high base mean) and because of their location at some distance from the diagonal line, reflecting differential expression in wt and $\alpha11^{-/-}$ FLS, even though not reaching statistically significant differences.

However, wt FLS showed a clearly differential response to damaged versus undamaged chondrocyte matrices, revealing 50 differentially expressed genes (DEG; |fold change| > 1.5 and adjusted p-value <0.05), illustrated by hierarchical clustering based on the most frequently identified transcripts (base mean > 300) (Fig. 5D). Amongst those transcripts, increased expression of macrophage metalloelastase *Mmp12* was detected in wt FLS on damaged matrix, which was confirmed by RT-PCR (Fig. 5E). Of note, we detected a sex-dependent difference in *Itga11* expression in 4 independent wt FLS samples upon contact with both, undamaged and damaged matrix (Fig. 5F). *Itga11* transcript levels were more than 3-fold higher in FLS isolated from male than from female mice. All data points together showed a high variability that presumably

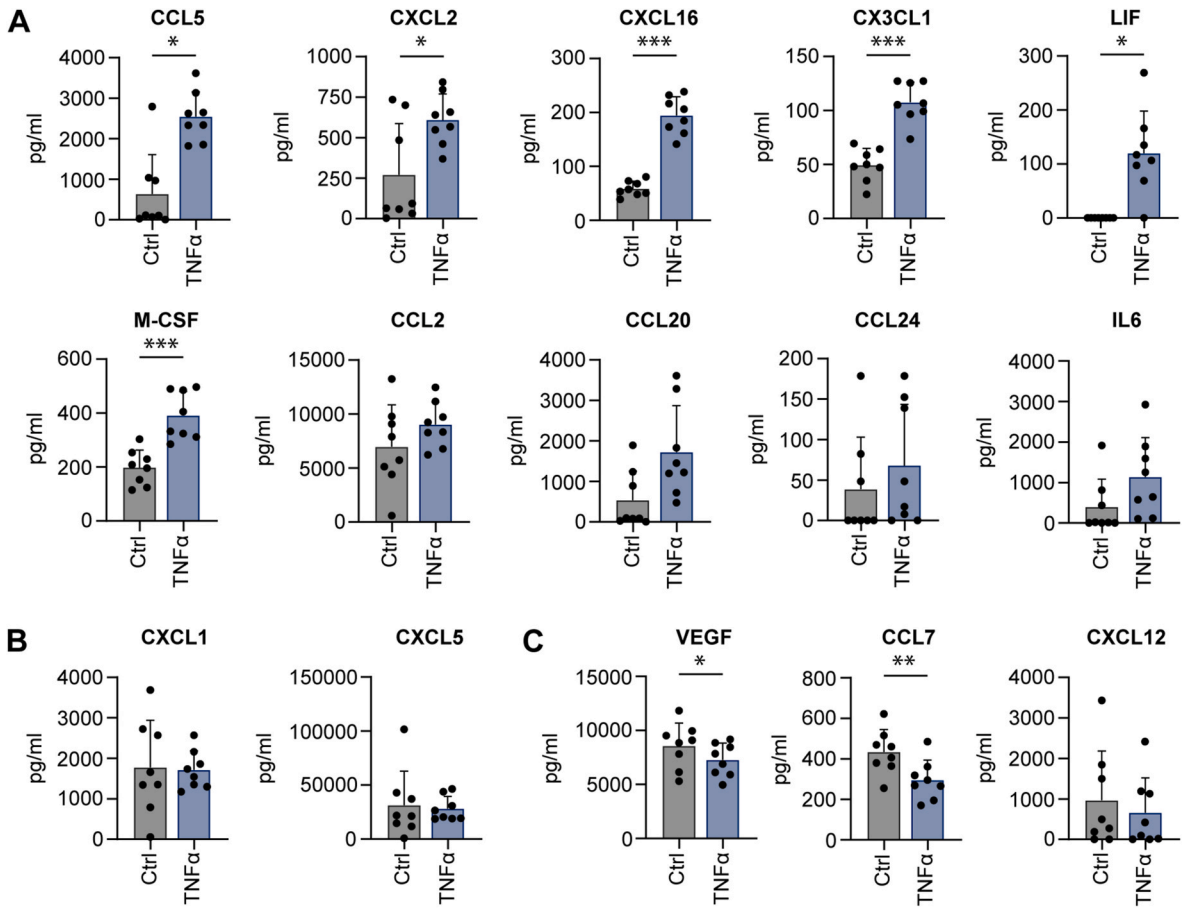

Fig. 3. Levels of soluble cytokines released by TNFα-treated and ctrl chondrocyte cultures. Bead-based analysis of cytokines in supernatants of chondrocyte cultures. Cultures were treated as shown in Fig. 1A until d14, when serum-free media were supplied and left for 48 h. Plotted values show concentration after subtraction of blank. Values below detection threshold are plotted as 0. **A.** Cytokines detected in part at significantly higher levels in TNFα-treated than ctrl cultures. **B.** Cytokines detected at comparable levels and **C.** Cytokines detected at reduced levels in TNFα-treated cultures. Significance of difference was calculated with paired Student's t-test for all cytokines except LIF, IL6, CCL5 for which Wilcoxon matched-pairs signed rank test was used. n = 8 per condition. *p < 0.05, **p < 0.01, ***p < 0.001.

accounted for the lack of statistically significant differences in overall *Itga11* transcript levels between FLS grown on damaged or ctrl matrices. The question then arose if TNFα that may have remained in the treated chondrocyte matrix might induce *Itga1*1 mRNA or protein. This was clearly not the case as demonstrated by western blotting for the α11 subunit of wt FLS cultures that were treated with the same concentration of TNFα as supplied to chondrocytes during the phase of matrix deposition (Fig. 5G). Therefore, *Itga11* transcript levels were induced in wt FLS by contact with a damaged chondrocyte matrix but not by TNFα, which provides a plausible explanation for the increased α11β1 protein detected in RA synovia of patients and hTNFtg mice.

While the results shown in Fig. 5B to D illustrate clear differences in the response of wt FLS to damaged versus undamaged chondrocyte matrices, no significant differences between wt FLS and $\alpha11^{-/-}$ FLS were detected.

Differences in release of soluble chemokines and cytokines by FLS grown on damaged or healthy chondrocyte matrices.

Since the culture of FLS on chondrocyte matrices may also affect the spectrum of soluble chemokines and cytokines that can act in an autocrine fashion, we also determined the cytokine profile secreted by FLS in response to different chondrocyte matrices in culture supernatants (Fig. 6). Most of the detected mediators tended to show increased levels released by FLS seeded on damaged than on undamaged matrix, without reaching statistical significance. This applied to both, wt and $\alpha11^{-/-}$ FLS. Of note, CCL19 was secreted at significantly lower amounts by $\alpha11^{-/-}$ compared to wt FLS. A similar pattern was also detected for CCL11. CCL5 stood out as it was below the detection level (lower limit of quantification = 1.08 pg/ml) in supernatants of wt or $\alpha11^{-/-}$ FLS seeded on undamaged chondrocyte matrix, but it was highly increased in cultures of wt, but not $\alpha11^{-/-}$, FLS grown on damaged matrix.

Overall, levels produced by $\alpha11^{-/-}$ FLS were lower than those released by wt FLS. Those differences between the two genotypes were seen in a number of chemokines (e.g. many CXCLs and CCL2) in the response to chondrocyte matrix. However, differences did not reach statistical significance, likely due to extensive variation between data points.

3. Discussion

We here asked the question of how a damaged extracellular matrix contributes to the activation of FLS that are the key cells in invasion and destruction of cartilage and bone in joints of RA patients. This question arose from the finding that the ECM in RA seems to be not only the target of activated FLS but also an activating trigger [8]. The mechanisms through which cartilage damage, within the context of other specific disease alterations, affects FLS, remain unclear. One potential explanation is that chondrocytes respond to inflammatory conditions by releasing factors that bind to the extracellular matrix (ECM). These factors may be released during cartilage damage, subsequently activating FLS, which in turn initiates additional interactions with ECM components. To address this question, we devised a simplified culture system in which articular chondrocytes deposit a dense ECM over the

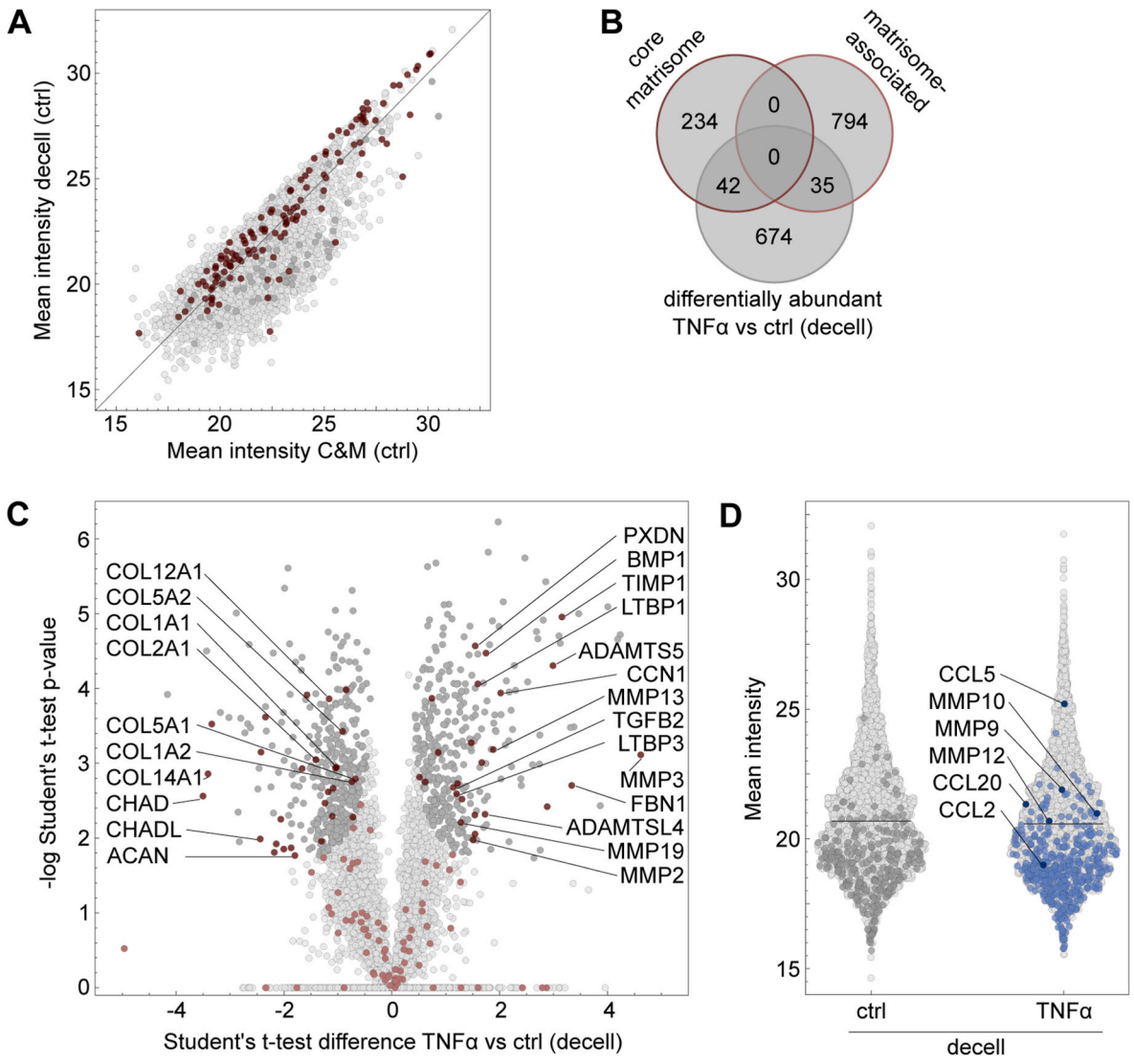

Fig. 4. Changes in the proteomes of TNFα-treated and ctrl chondrocytes. Cultures were treated as shown in Fig. 1A and subjected to proteomic analysis either at d14 prior to decellularization (cells plus matrix, C&M) or at d15 after decellularization, showing deposited matrix only. **A**. Scatter plot showing the mean intensity of all identified proteins in C&M ctrl against decellularized (decell) ctrl. ECM proteins are highlighted in red, actin cytoskeleton proteins in dark grey. **B**. Venn diagram showing the numbers of regulated core matrisome and matrisome-associated proteins in decellularized matrices of TNFα-treated versus ctrl cultures. **C**. Volcano plot showing Student's t-test difference against Student's t-test p-value. Significantly changed proteins (permutation-based false discovery rate <0.01) are highlighted in dark grey. ECM proteins are highlighted in red, significantly different ones are shown in dark red. **D**. Swarm plot showing the mean intensity of all identified proteins in the decellularized matrices of ctrl and TNFα-treated chondrocytes. Proteins identified solely in decellularized untreated (ctrl) matrices are highlighted in dark grey, proteins only found in decellularized TNFα-treated matrices are highlighted in blue. Horizontal line represents median. n = 4 per condition.

course of 2 weeks. To generate an RA-like matrix, TNFα was added to chondrocytes depositing ECM. Chondrocytes and TNFα were then removed and the deposited matrix was left to be seeded with FLS. Using this culture model, we aimed to (a) identify the composition and differences in ECM deposited by TNFα-treated (RA-like) versus healthy chondrocytes; (b) determine how the RA-like versus healthy ECM influences the phenotype of FLS; and (c) show how the presence or absence of integrin α11β1 in FLS influences the FLS response to the damaged matrix.

TNFα treatment of chondrocytes resulted in significantly induced transcription of a large number of genes, in particular those encoding ECM-degrading enzymes and some inflammation-related cytokines, while at the same time reducing critical cartilage components such as aggrecan, COMP and several collagens including collagens II, IX and XI. These RNA seq results were confirmed by mass spectrometric analyses of the deposited ECM only, demonstrating that the continued presence of TNFα, one of the most potent pathogenic stimuli in RA patients, assists in generation of an *in vitro* ECM with characteristic features seen in patients' joints [11,23–25]. The RA-like matrix is characterized in particular by the altered abundance of 42 proteins associated with the core matrisome and 35 proteins assigned to the matrisome-associated group, clearly demonstrating extensive changes in ECM composition. In addition to the loss of structural proteins, the identification of MMPs −9, −10 and −12, enzymes with a broad spectrum of extracellular matrix substrates, which we detected uniquely in the RA-like ECM, further underscored the large extent of remodeling and alteration of the damaged matrix. All three MMPs are known to be induced by TNFα through the NFkB pathway [26,27], and MMPs can modulate the expression or activation of other MMPs, giving rise to a complex degrading environment. Moreover, MMPs have functions beyond degrading matrix, such as releasing ECM fragments that may exert activities that differ from those of the uncleaved parental protein [28,29]. The detection of such ECM cleavage products is difficult using mass spectrometry and requires methods such as degradomics, which is

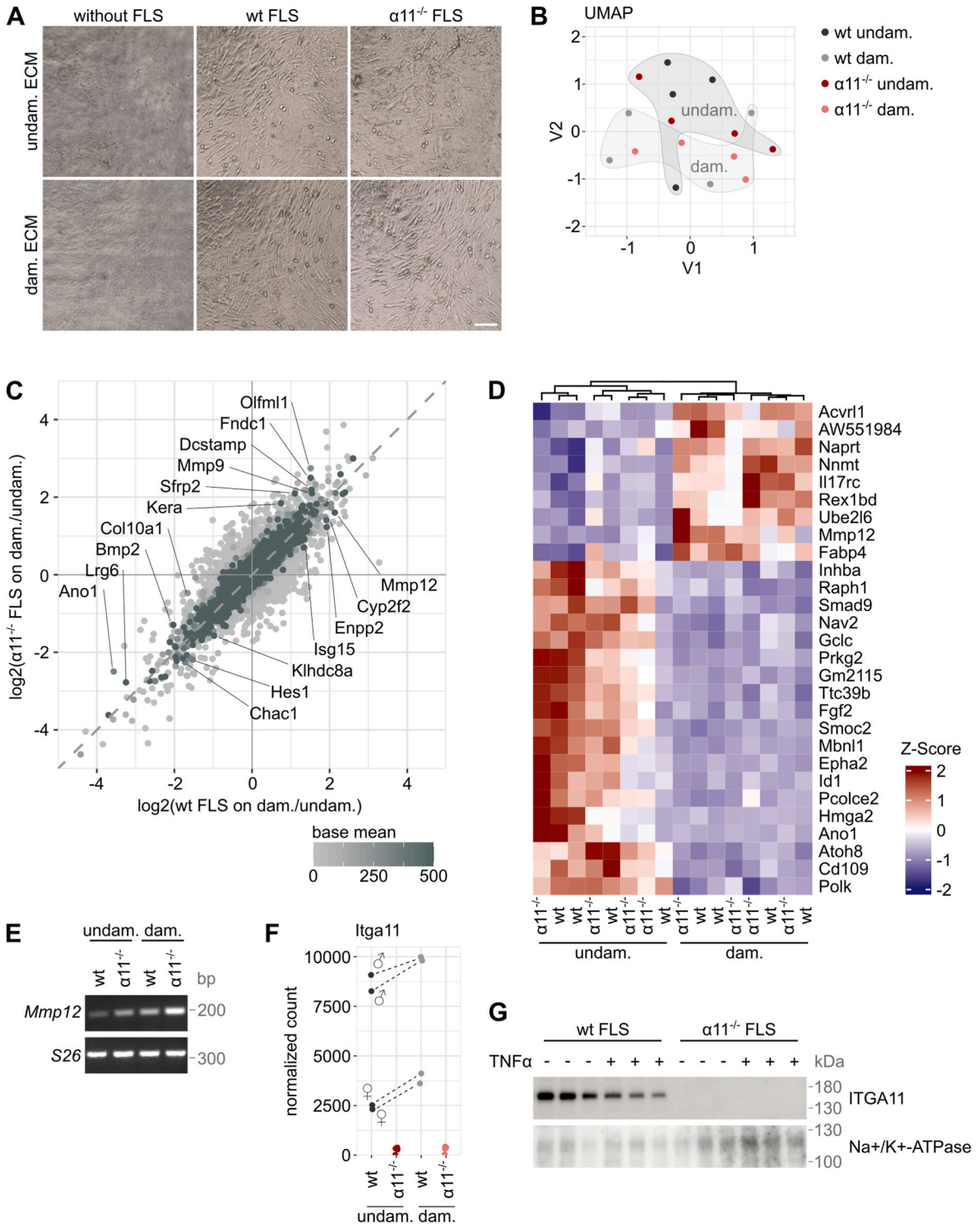

Fig. 5. Transcriptional changes in FLS induced by chondrocyte matrices. Chondrocyte cultures were set up as shown in Fig. 1A in the absence or presence of TNFα to generate undamaged and damaged ECM, respectively. Cultures were treated to remove chondrocytes, and decellularized matrices were seeded with FLS from wt or $\alpha11^{-/-}$ FLS for 72 h. **A.** Morphology of wt and $\alpha11^{-/-}$ FLS on undamaged or damaged chondrocyte matrices. Scale bar: 100 μm. **B-D.** RNA-seq data analysis of FLS on chondrocyte matrices. **B.** UMAP showing the segregation of the four FLS samples. **C.** Scatter plot showing the expression ratio between wt FLS on damaged versus undamaged matrix against the ratio of $\alpha11^{-/-}$ FLS on damaged versus undamaged matrix. Ratios are plotted as log2 values. **D.** Hierarchical clustering showing the z-transformed expression values of the most frequently identified DEG (base mean > 300) of the main effect, which is the condition effect (damaged versus undamaged matrix) for wt FLS. **E.** RT-PCR verifying induced *Mmp12* expression in FLS grown on a damaged chondrocyte matrix. **F.** Matrix-dependent increase in *Itga11* transcripts showing gender-dependent differences. Values for cells derived from male mice (♂) show higher normalized counts than females (♀), revealed by RNA-seq analysis. **G.** Western blot of FLS cultured on tissue culture plastic for 24 h in the absence or presence of 100 ng/ml TNFα. Crude membrane preparations were probed for ITGA11, the α11 subunit of integrin α11β1. Na/K-ATPase was used for normalization. n = 4 per condition in B-D and F, n = 2 in A and E, n = 3 in G.

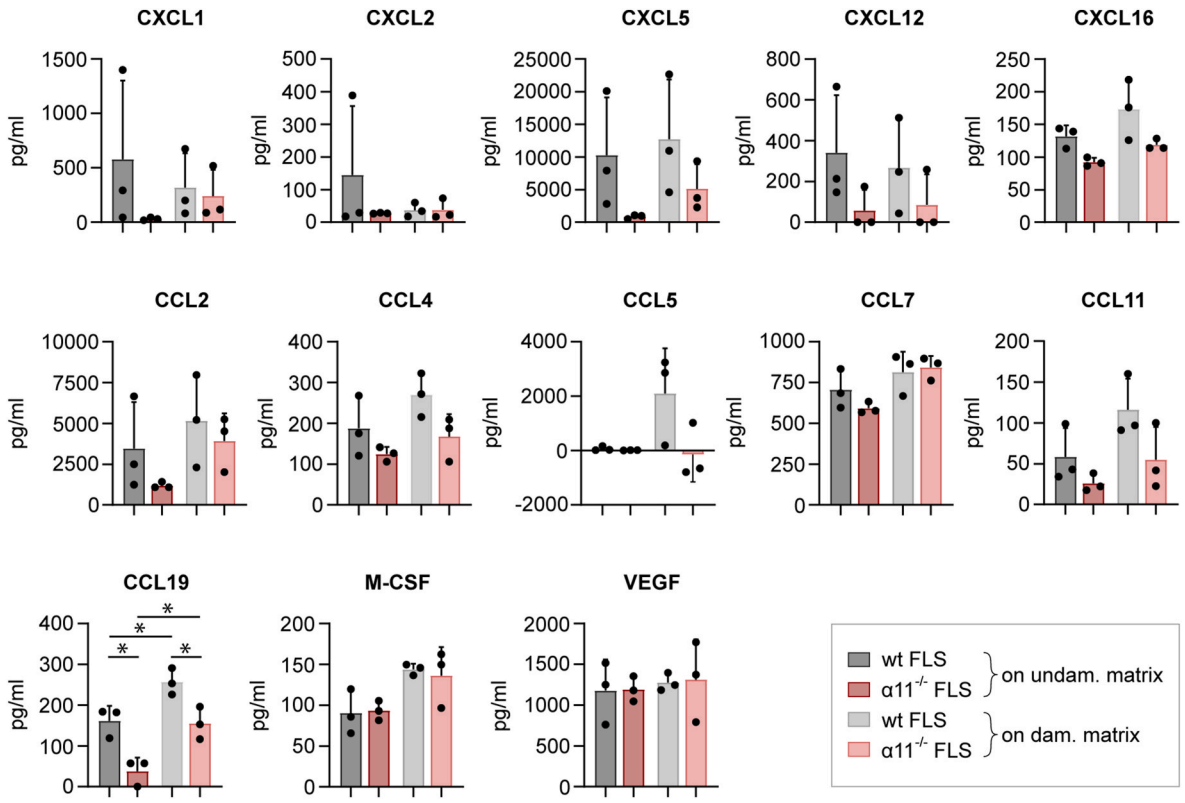

Fig. 6. Levels of soluble chemokines and cytokines released by FLS grown on TNFα-treated or ctrl chondrocyte matrices. Cultures were set up as described in Fig. 1A and seeded with either wt or $\alpha11^{-/-}$ FLS for 72 h. Culture media were changed (on d17 in Fig. 1A) to serum-free media 24 h before harvest (on d18) and subjected to bead-based assays. Plotted values show concentration after subtraction of blank. Values below detection threshold are plotted as 0. Significance of difference was calculated using two-way ANOVA with Šídák's multiple comparisons test. *$p < 0.05$. $n = 3$ per condition.

capable of detecting protease-generated neo-N termini of the cleaved fragments and thereby of discriminating between full-length and cleaved fragments of proteins [30]. Vice versa it was shown that an aggrecan fragment stimulates *Mmp12* expression in murine chondrocytes and FLS [31]. Some MMPs, including MMP12, have been implicated in modulating inflammatory responses by both, aggravating or attenuating the inflammatory response [32,33].

Interestingly, we detected chemokines such as CCL2, -5 and -20 by mass spectrometry of the matrix, indicating that they are bound by the deposited chondrocyte matrix and present in high abundance. CCL2 and -5 are known to be secreted in RA patients and have been associated with disease severity [34]. In addition to those matrix-embedded chemokines, we also identified soluble mediators released to chondrocyte media, which altogether contribute to an inflammatory environment like that present in RA tissue [21]. Of interest, we detected CXCL16 and CX3CL1 at significantly increased levels in supernatants of TNFα-treated chondrocytes, which indicates that they were cleaved from their membrane-spanning version to generate soluble, active forms. This can be accomplished by ADAM10 or -17 [35], both of which were found increased in damaged matrix. Cleaved, soluble forms of CXCL16 and CX3CL1 are chemoattractant for immune cells including leukocytes [35,36], which indicates that in the presence of TNFα, chondrocytes actively contribute to the recruitment of immune cells and to the generation of an inflammatory environment.

While the culture model used here reflects many characteristics seen also in RA patients or mouse models, there are some differences. Examples include upregulation of CCL7 in patients [37], which was downregulated in our cytokine assays, as well as upregulation of CXCL1, CXCL5 and CXCL12 in patients [34], which we detected at comparable levels in treated and control cultures. These differences may be explained by the presence of additional cell types *in vivo*, in particular macrophages and further immune cells, but their absence in our cultures.

Together, our study has dissected in detail the components of an *in vitro* generated RA-like matrix that reflects the characteristic loss of ECM structural proteins in RA and is rich in ECM remodeling and degrading enzymes as well as inflammatory mediators. Based on these findings, we use the term 'damaged matrix' although strictly speaking we here describe a matrix with an RA-like catabolic, inflammatory signature, while the presence of cleaved ECM fragments remains to be demonstrated.

Which response does the RA-like matrix evoke in FLS in comparison to a healthy chondrocyte matrix? Transcriptome and cytokine analyses revealed that FLS show a distinctly different response to the damaged chondrocyte matrix. That of wt FLS to a damaged matrix is characterized by increased *Mmp12*, which is also increased in patient synovial tissue [38] and which induces more severe arthritis in MMP12 overexpressing rabbits [31]. Induced *Mmp12* expression can be caused by aggrecan fragments in the damaged matrix, as discussed above. This alteration points to a matrix degradation and remodeling response in the FLS. Moreover, increased expression of *Nnmt* (nicotinamide N-methyltransferase) in FLS grown on a damaged matrix depicts similarities with cancer-associated fibroblasts [39,40] and supports the shared aggressive and invasive phenotype of cancer-associated fibroblasts and FLS, postulated by some of us previously [41]. In addition, matrix maturation seems to be negatively affected as indicated by reduced expression of genes involved in matrix organization, including *Fgf2* (fibroblast growth factor-2), *Pcolce2* (procollagen C-endopeptidase enhancer-2), *Lamb3* (laminin beta3) [42–44].

On the other hand, *Gdf6* (growth differentiation factor 6) was upregulated by the contact of wt FLS with damaged matrix. This factor is described to induce chondrogenesis by increased production of collagen

II and aggrecan [45]. In contrast to the matrix degrading and impaired maturation phenotype discussed above, this finding suggests that the FLS adapt to the altered conditions by initiating a repair response.

Furthermore, FLS seeded on damaged matrix expressed elevated levels of interleukin receptors *Il17rc* and *Il1r2*. Heteromeric interleukin receptor IL17RA/RC, but also IL17RC alone, binds to IL17A and IL17F, which are increased in synovial fluid of RA patients and other autoimmune diseases [46]. Therefore, the IL17 pathway has become a major therapeutic target in autoimmune diseases [47]. These findings support an active role of FLS in maintaining or amplifying an inflammatory process. In contrast, the non-signaling receptor IL1R2 binds IL1 and thereby inhibits IL1 signaling in macrophages, leading to attenuated collagen-induced arthritis in mice [48]. Therefore, increased expression of those interleukin receptors by FLS on damaged chondrocyte ECM suggests a defense mechanism of the cells to their pathological environment. By increasing the IL1R2 expression, FLS might counteract a further inflammatory response to interleukin signaling.

The analysis of soluble cytokines and chemokines revealed significantly increased secretion of CCL19 by FLS seeded on damaged matrix. CCL19 expression by FLS of RA patients has indeed been reported [34]. Moreover, analysis of fibroblast heterogeneity has demonstrated a fibroblast subset that is expanded across a variety of inflammatory diseases including RA, which is characterized by high expression of CXCL10 and CCL19 upon activation by cytokines. Those fibroblasts were designated as immune-interacting fibroblasts [49], since CCL19 acts as a chemoattractant for dendritic cells, lymphocytes and monocytes [34,50,51]. Those data indicate that the interaction of FLS with a damaged chondrocyte matrix can induce an immune-interacting phenotype in FLS, which attracts immune cells into the synovial joint. This notion agrees with our result that secretion of the chemokines CCL7, CXCL16 and M-CSF, all known to be expressed in several tissues of RA patients and to act as chemoattractants for monocytes and leukocytes [34], were increased in FLS in contact with damaged matrix. This suggests that FLS in contact with a damaged chondrocyte matrix contribute to sustaining an inflammatory environment, presumably by cell-cell interaction with immune cells that can induce an accelerated inflammatory response.

Our study did not reveal major differences between the responses to a damaged matrix of FLS with or without integrin α11β1, with one exception: $\alpha11^{-/-}$ FLS secreted less CCL11 and CCL19 compared to wt FLS. We observed that CCL11 is expressed only by FLS grown on matrices produced by chondrocytes, while there is no expression in FLS grown on tissue culture plastic (not shown). Its expression was detected in FLS on healthy chondrocyte matrices but elevated by contact with a damaged matrix. CCL11 was shown to be present at elevated levels in synovia of RA patients and to stimulate FLS migration [50]. CCL19, also released at significantly lower levels by $\alpha11^{-/-}$ than wt FLS, was significantly induced in both FLS by contact with a damaged matrix. CCL19 was also reported to be expressed by RA-FLS [34] and was attributed a role in attracting immune cells [52]. Taking into account our finding that α11β1 itself is induced in FLS by contact with the damaged matrix. These results provide an explanation for the reduced disease severity in mice lacking integrin α11β1: FLS without this collagen-binding integrin have a reduced capacity for invasive migration in the affected tissues and for interacting with immunocompetent cells.

4. Experimental procedures

4.1. Cells and culture

Primary epiphyseal chondrocytes (PEC) were isolated from newborn C57BL6/N mice (postnatal day 1–3). Newborns were sacrificed by decapitation and dissected tibial and femoral epiphyses were digested with collagenase P (PEC medium: DMEM/F12, cat no. 10565018, Thermo Fisher Scientific/Gibco™; 10 % FBS, cat no. 10270-106, Thermo Fisher Scientific/Gibco™; 1 % Penicillin-Streptomycin, cat no. P0781, Merck/Sigma-Aldrich; supplemented with 1.61 U/ml collagenase P, cat no. 11213865001, Merck/Roche; 175.5 μg/ml L-cysteine hydrochloride, cat no. C1276, Merck/Sigma-Aldrich) for 18.5 h at 37 °C. Cells from 3 to 6 mice were pooled and resuspended in PEC medium. Cells were passed sequentially through cell strainers of 100 μm and 40 μm pore size. Chondrocytes were resuspended in PEC medium containing ascorbic acid (final concentration: 0.25 mM ascorbic acid, cat no. A4544, Merck/Sigma-Aldrich; 0.45 mM ascorbic acid-2-phosphate, cat no. A8960, Merck/Sigma-Aldrich), and 50,000 cells in 80 μl medium were seeded on tissue culture plastic in one chamber of culture inserts (Ibidi, cat no. 80209) (day 0). From day 1, 10 ng/ml TGFβ3 (cat no. 8420-B3, R&D Systems, Inc.) was added to the culture medium. The medium was changed every other day. To generate damaged matrix, cells were treated with 100 ng/ml TNFα (cat no. 210-TA, R&D Systems, Inc.) from day 4. Cells and deposited matrices were collected on day 14 and used for further experiments, as indicated in the figure legends. All mouse work was approved by the local animal welfare agencies (LANUV NRW 81-02.05.40.18.014 and UniKöln_4.20.030).

After 14 days in culture, deposited chondrocyte matrices were decellularized. Cultures were washed with PBS (Thermo Fisher Scientific/Gibco™) once and decellularized by three freezing/thawing cycles. Cultures were frozen for 20 min at −80 °C (twice dry, once in 10 mM Tris-HCl, pH 6.8, cat no. 1610799, Bio-Rad Laboratories) and thawed by submerging in prewarmed PBS and incubation for 20 min at 37 °C. Cultures were washed in Tris-HCl (10 mM, pH 6.8) overnight at 4 °C on a rocking platform shaker and three more times for 3 min each with PBS before immediate use.

Primary fibroblast-like synoviocytes (FLS) were isolated from 10 to 13 weeks old C57BL6/N or $Itga11^{-/-}$ mice [16]. Mice were sacrificed by cervical dislocation. Skin, tendons, claws and nerves were removed from the hind paws and remaining tissue containing the synovia was digested in DMEM (cat no. 41965, Thermo Fisher Scientific/Gibco™) supplemented with collagenase type 4 (160 U/ml, cat no. LS004189, Worthington) for 1.5 h at 37 °C with stirring. Liberated cells were collected by centrifugation (160×*g*, 5 min, RT) and seeded in FLS medium (DMEM, cat no. 41965, Thermo Fisher Scientific/Gibco™; 10 % FBS, cat no. 10270-106, Thermo Fisher Scientific/Gibco™; 1 % Penicillin-Streptomycin, cat no. P0781, Merck/Sigma-Aldrich). Cells were used at passage 3 or 4.

To investigate the response of FLS to chondrocyte matrices, FLS were seeded on decellularized chondrocyte matrices deposited as described in PEC medium with ascorbic acid. 10,000 FLS isolated from one mouse were seeded in one chamber of the culture insert.

4.2. Genotyping

Genomic DNA was isolated from ear punch biopsies or cultured FLS and subjected to PCR analysis using the following primers: ITGA11 wt forward 5′- CCA TCA GAA GAC AGG AGA CG -3′, ITGA11 wt reverse 5′- TGG TCA GTG GAT GGG TTA GGA AG -3’ (688 bp), ITGA11-LacZ forward 5′- GTG GTG GTT ATG CCG ATC GC -3′, ITGA11-LacZ reverse 5′- TAC CAC AGC GGA TGG TTC GG -3’ (352 bp). The PCR was performed according to the following program: Initial activation 6 min, 94 °C; denaturation 30 s, 94 °C; annealing 45 s at 52 °C; elongation 60 s (35 cycles), 72 °C; dissociation 5 min, 72 °C. Amplified products were resolved by agarose gel electrophoresis and visualized using Gel Doc™ EZ Imager (BioRad).

4.3. RNA isolation

Total RNA was isolated using RNeasy® Plus Micro Kit (cat no. 74034, Qiagen) and RNeasy® Fibrous Tissue Mini Kit (cat no. 74704, Qiagen) for FLS and chondrocytes, respectively. The cells were washed with PBS and scraped into 350 μl RLT buffer containing 2-mercaptoethanol (10 μl/ml, Merck KGaA). Deposited matrix was homogenized through high-speed shaking of the sample with a stainless steel bead (cat. no. 69989,

Qiagen) using TissueLyser II (Qiagen) for 2 min at 25 Hz/s. Subsequently, RNA was isolated according to the manufacturer's protocol. RNA was eluted in nuclease-free water and the concentration was determined by NanoDrop™ One (Thermo Fisher Scientific/Thermo Scientific™).

4.4. cDNA synthesis and semi-quantitative reverse transcription PCR (RT-PCR)

cDNA was synthesized using RevertAid First Strand cDNA Synthesis Kit (cat no. K1622, Thermo Fisher Scientific/Thermo Scientific™) according to the manufacturer's protocol.

Levels of mRNA of genes of interest were determined by semi-quantitative reverse transcription PCR (RT-PCR). The cDNA served as template for PCR according to the following programs with specific primers: Initial activation 7 min, 95 °C; denaturation 30 s, 94 °C; annealing 30 s at 55–59 °C (depending on target); elongation 45 s, 72 °C; dissociation 5 min, 72 °C. The following primer combinations were used: *Acan* forward 5′- AGG TGG TAC TGC TGG TGG C -3′, *Acan* reverse 5′- CGT AGG TTC TCA CTC CAG GG -3' (453 bp); *Cilp2* forward 5′- CTA TGG CGT CTA CAC GGT CAC -3′, *Cilp2* reverse 5′- TGT CTC CAG CCT GGG TTT G -3' (271 bp); *Col2a1* forward 5′- CTG CAG GTG AAC AAG GAC CC -3′, *Col2a1* reverse 5′- CTC TGT GAC CCT TGA CAC CG -3' (495 bp); *Mmp3* forward 5′- TGGAGATGCTCACTTTGACG -3′, *Mmp3* reverse 5′- GCCTTGGCTGAGTGGTAGAG -3' (120 bp); *Mmp9* forward 5′- CAT TCG CGT GGA TAA GGA GT -3′, *Mmp9* reverse 5′- ATT TTG GAA ACT CAC ACG CC -3' (118 bp); *Mmp12* forward 5′- CTG CTC CCA TGA ATG ACA GTG -3′, *Mmp12* reverse 5′- AGT TGC TTC TAG CCC AAA GAA C -3' (158 bp); *Mmp13* forward 5′- TCC ACA GTT GAC AGG CTC CG -3′, *Mmp13* reverse 5′- GAA ACA TCA GGG CTC CTG GG -3' (538 bp); *Prg4* forward 5′- GTG GAT GAA GCT GGA AGC GG -3′, *Prg4* reverse 5′- GTT GGA GGT GGT TCC TTG GG -3' (443 bp); *S26* forward 5′- AAT GTG CAG CCC ATT CGC TG -3′, *S26* reverse 5′- CTT CCG TCC TTA CAA AAC GG -3' (324 bp). Amplified products were resolved by agarose gel electrophoresis and visualized under UV light using a Gel Doc™ EZ Imager (BioRad).

4.5. Bulk RNA sequencing (RNA-seq)

Libraries were prepared using the Illumina® TruSeq® RNA Sample Preparation Kit. Library preparation was started with 500 ng total RNA. After poly-A selection (using poly-T oligo-attached magnetic beads), mRNA was purified and fragmented using divalent cations under elevated temperature. The RNA fragments underwent reverse transcription using random primers. This is followed by second strand cDNA synthesis with DNA Polymerase I and RNase H. After end repair and A-tailing, indexing adapters were ligated. The products were then purified and amplified (15 PCR cycles) to create the final cDNA libraries. After Library validation and quantification (Agilent 4200 TapeStation System and Qubit™ dsDNA BR-Assay-Kit), equimolar amounts of Library were pooled together. The pool was quantified by using the Roche KAPA Library Quantification Kit and the Applied Biosystems 7900HT Sequence Detection System. The pool was sequenced by using an Illumina NovaSeq XP 4-Lane Kit v1.5 and the Illumina NovaSeq 6000 S4 Reagent Kit v1.5 (101 + 10+10 + 101 Cycles) on an Illumina NovaSeq 6000 Sequencer.

4.6. RNA-seq data analysis

Pre-processing, genome alignment and post-processing of the files were performed on the Cologne High Efficiency Operating Platform for Science (CHEOPS). Subsequent statistical analysis of the results was done with R 4.2.3 [53] using R Studio 2023.03.0 + 386 [54]. To eliminate adapter sequences, adapter trimming and quality filtering was performed with Cutadapt 4.1 [55]. Since insufficient numbers of reads were generated in the first run for some samples, those samples were sequenced a second time to obtain approximately 50 million reads in total. Results of the first and second runs were merged into one file after adapter trimming (`cat file1 file2 > file_merged`). A high quality of trimmed files was confirmed with FastQC 0.11.9 (https://www.bioinformatics.babraham.ac.uk/projects/fastqc/). For alignment, STAR 2.7.8 [56] with default settings was used to generate a reference genome using genome sequence, primary assembly GRCm39 and the comprehensive gene annotation vM30 (https://www.gencodegenes.org/mouse/). Subsequently, STAR with default settings was used for alignment of the trimmed files to the generated reference genome. Count tables were created with the featureCounts [57] function from Subread v2.0.1 [58]. For subsequent statistical analysis and visualization of the results, different R packages were used: ggplot2 3.4.2 [59], ggh4x 0.2.4 [60], ggrepel 0.9.3 [61], circlize 0.4.15 [62], stringr 1.5.0 [63], dyplr 1.1.1 [64], DESeq2 1.38.3 [65], org.Mm.eg.db 3.16.0 [66], uwot 0.1.14 [67], rrcov 1.7–2 [68], ComplexHeatmap 2.14.0 [69,70], clusterProfiler 4.7.1.003 [71], svglite 2.1.1 [72]. Low abundance transcripts with an overall mean below the threshold (five times the number of samples) were removed and a two-dimensional Uniform Manifold Approximation and Projection (UMAP) embedding was created [73]. Calculation of the normalized counts was performed according to the DESeq2 standard analysis workflow. For the transcriptome of chondrocytes, normalized counts were obtained from the multiple-testing-corrected (Benjamini--Hochberg) DESeq2 results using an alpha-level of 0.05 and log2 fold change threshold of 0.6. For FLS grown on chondrocyte matrices, normalized counts were obtained in the same way, except a log2 fold change threshold of 0 was used. Overall representation analysis for KEGG (Kyoto Encyclopedia of Genes and Genomes) pathways were performed with clusterProfiler using default settings.

4.7. Protein extraction and western blotting

Cells along with their deposited matrix were harvested by scraping and were shock frozen in liquid nitrogen. For Western blot, pellets were homogenized with stainless steel beads in TissueLyser II (Qiagen; 2 min, 25 Hz/s) and lysed in Cell lysis buffer (50 mM Tris-HCl pH 7.5, SERVA Electrophoresis GmbH; 1 % SDS, ITW Reagents Division; 0.5 % NP40, Fluka BioChemika; 2 mM EDTA, VWR International, LLC, in aqua dist.) or RIPA (25 mM Tris-Cl, pH 7.5, 150 mM NaCl, 1 % Triton-X100; 0.1 % SDS) supplemented with protease inhibitor (cat no. P8340, Merck KGaA/Sigma-Aldrich). Cells were further disrupted by sonication in an ultrasonic bath (Branson Sonifier 450; 20 impulses, 80 % duty cycle, output control 8). Lysates were stored at −80 °C.

To determine levels of surface-localized integrins, membranes were isolated. Cells were washed, scraped off the plate in 1 ml PBS with a cell scraper and collected by centrifugation (160×*g*, 5 min, RT). The pellet was resuspended in 150 µl sucrose lysis buffer (50 % sucrose, Carl Roth GmbH + Co. KG; 48 mM HEPES, Serva Electrophoresis GmbH; 0.1 M EDTA, VWR International, LLC; 5 mM EGTA, Carl Roth GmbH + Co. KG; in aqua dist.) and cells were disrupted by three cycles of freezing/thawing in liquid nitrogen and a water bath set at 37 °C. Intact cells were removed by centrifugation (160×*g*, 3 min, 4 °C). The supernatant was centrifuged (16,000×*g*, 10 min, 4 °C) to collect the cell membranes. The pellet was resuspended in 50 µl PBS supplemented with protease inhibitor (cat no. P8340, Merck KGaA/Sigma-Aldrich).

Cell lysates were denatured with loading buffer and heated for 5 min at 95 °C. Proteins were separated by SDS-polyacrylamide gel (5 % Stacking gel: 415 µl Rotiphorese® gel 30, Carl Roth GmbH + Co. KG; 315 µl Tris-HCl 0.5 M pH 6.8, cat no. 1610799, Bio-Rad Laboratories; 25 µl SDS 10 %, ITW Reagents Division; 12.5 µl APS 20 %, Thermo Fisher Scientific/Invitrogen™, 2.5 µl TEMED, Carl Roth GmbH + Co. KG; 1.73 ml H_2O. 7.5 % Separation gel: 2.5 ml Rotiphorese® gel 30, Carl Roth GmbH + Co. KG; 3.5 ml Tris-HCl 1 M pH 8.8, SERVA Electrophoresis GmbH; 100 µl SDS 10 %, ITW Reagents Division; 50 µl APS 20 %, Thermo Fisher Scientific/Invitrogen™; 6 µl TEMED, Carl Roth GmbH + Co. KG; 3.84 ml H_2O) electrophoresis (15 min at 50 V, about 1.5 h at 100 V) and transferred to methanol-activated PVDF membranes (Merck

Millipore cat. no. IPVH00010; o/n, 100 mA, 4 °C) in a tank blotting chamber in transfer buffer (25 mM Tris base, Thermo Fisher Scientific/Invitrogen™; 0.2 M glycine, Carl Roth GmbH + Co. KG; 20 % methanol, Diagonal Münster; in aqua dest.). Successful transfer and equal loading of the samples were confirmed by Ponceau S staining (Merck KGaA/Sigma-Aldrich). To block unspecific binding sites, the membrane was incubated in ROTI®Block (Carl Roth GmbH + Co. KG) or 5 % milk powder (Carl Roth GmbH + Co. KG) in TBS (ITW Reagents Division) for 45 min at room temperature. First and secondary antibodies were diluted in TBS and incubated for 1 h at room temperature, each. Washing steps after Ponceau S staining and antibody incubations were performed with TBS-T (1x TBS buffer with 0.1 % Tween-20, Merck KGaA/Millipore). Signals were detected with SuperSignal™ West Pico PLUS Chemiluminescent Substrate (Thermo Fisher Scientific/Thermo Scientific™) in Amersham ImageQuant™ 800 (Cytiva).

The following antibodies were used for western blotting: rabbit anti-ACAN (AB1031, Millipore; 1:1000); goat anti-COL I (1310-01, SouthernBiotech, 1:2000); rabbit anti-COL II (ab34712, Abcam, 1:500); rabbit anti-COMP (AP1007, Immundiagnostik, 1:1000 [74]; rabbit anti-GAPDH (ab9485, Abcam, 1:2500); mouse anti-GAPDH (MAS15738, Thermo Fisher Scientific, 1:2000); rabbit anti-ITGA11 (Popova et al., 2007, 1:400); rabbit anti-Na+/K + ATPase (MAB25381, R&D systems, 1:5000); rabbit anti-goat immunoglobulins/HRP (P0449, Dako, 1:3000); swine anti-rabbit immunoglobulins/HRP (P0399, Dako, 1:3000); goat anti-rabbit immunoglobulins/HRP (P0399, Agilent, 1:3000); goat anti-mouse immunoglobulins/HRP (P0260; Agilent, 1:1000).

4.8. Chemokine and cytokine assays

Serum-free supernatants were collected, centrifuged (16,000×*g*, 10 min, 4 °C), transferred into a new tube and stored in aliquots at −80 °C until further use. To detect cytokines and chemokines, a magnetic bead-based multiplex immunoassay was performed. Bio-Plex Assays from Bio-Rad (Bio-Plex Pro Mouse Chemokine Panel 31-Plex #12009159; Bio-Plex Pro Mouse Cytokine 9-Plex Assay #MD000000EL; Bio-Plex Pro Mouse Cytokine IL-1α Set #171G5001M; Bio-Plex Pro Mouse Cytokine IL-33 Set #171GA009M; Bio-Plex Pro Reagent Kit V with Flat Bottom Plate #12002798; Bio-Plex Pro Mouse Th17 Cytokine Standards #171IA0001; Bio-Plex Pro Mouse Cytokine Standards Group I #171I50001; Bio-Rad Laboratories, Inc.) were used on a Bio-Plex 200 System with a Bio-Plex Pro Wash Station. By using the median of the fluorescence intensity and the standard curve, the absolute concentration of the cytokines (pg/mL) was calculated (Bio-Plex Manager 6.1, Bio-Rad Laboratories).

4.9. Sample preparation for mass spectrometry analysis

Cells or matrices were lysed in 4 % SDS/PBS and heated for 10 min at 95 °C with shaking (1400 rpm). Sonication of the samples was performed by ten cycles at 30 s intervals using a Bioruptor® Pico (Diagenode) and for 30 s at 8 s pulse using a sonicator with probe. Samples were again heated for 5 min at 95 °C shaking (1400 rpm) and cell debris was removed by centrifugation (18,000×*g*, 15 min, RT). Supernatants were transferred into new tubes and total protein amount was determined using Pierce™ Rapid Gold BCA Protein Assay Kit according to the manufacturer's protocol. Samples were diluted to 8 µg in 30 µl 4 % SDS. Cysteine reduction and alkylation was achieved by addition of TCEP (Tris(2-carboxyethyl)phosphine hydrochloride, 5 mM final concentration) and CAA (chloroacetamide, 40 mM final concentration) for 10 min at 70 °C. Protein lysates were digested using the single-prot, solid-phase-enhanced sample preparation [75]. In brief, 20 mg of magnetic hydrophilic and hydrophobic carboxy beads were added to the samples and mixed with 1× sample volume of acetonitrile (ACN). After washing with 70 % ethanol twice, and once with CAN, samples were digested with LysC (1:200 enzyme:substrate) and trypsin (1:100 enzyme:substrate) in 10 µl ammonium bicarbonate (50 mM) overnight at 37 °C. Peptides were cleaned up with in-house made double-layer SDB-RPS stage tips.

4.10. LC-MS/MS analysis

Purified peptides were reconstituted in 2 % ACN, 5 % formic acid. Peptides were separated using an in-house made 30 cm fused silica emitter (75 µm diameter), packed with 5 µm C18 Poroshell resin (Agilent, USA) and applied to an Easy nLC1200 (Thermo-Fisher Scientific, Waltham, USA) with the column temperature maintained at 50 °C using an integrated column oven. For Solvent A 0.1 % FA and for Solvent B 80 % acetonitril, 0.1 % FA was used. A 90 min segmented gradient of 4–32 % Solvent B over 72 min, 32–55 % Solvent B over 13 min and 55–95 % over 2 min at a flow rate of 300 nl/min was applied to elute peptides and measured with an Orbitrap Eclipse Tribid (Thermo-Fisher Scientific, Waltham, USA) equipped with an FAIMS.Pro interface (Thermo-Fisher Scientific, Waltham, USA). A single CV of −50V was selected during peptide ionization, to reduce background noise from uncharged peptides. A data-independent acquisition method was used with staggered windows, employing a duty cycle of 2 sets of DIA acquisitions shifted by ½ isolation window from 400 to 1050 *m/z* with a resolution of 15k. DIA scans were performed at a resolution of 15k, employing a 30 × 20 Da windows from 350 to 1600 *m/z*.

4.11. Bioinformatics LC-MS/MS analysis

The mass spectrometry proteomics data have been deposited to the ProteomeXchange Consortium via the PRIDE partner repository with the dataset identifier PXD049800 [76]. For tissue analysis thermo raw files were first unstaggered using ProteoWizard (V 3.0.21218). Files were processed with DIA-NN 1.8.1 using a library-free search against UniProt mouse database (Sep. 2017) complemented with protein sequences from collagens [77]. Mass ranges were set according to the settings of the mass spectrometer, mass deviation was automatically determined from the first data file. Data were further processed using R (V 4.2.2), with the libraries: tidyverse, diann, data.table, magrittr, FactoMineR, factoextra and ggplot2, gprofiler. An in-house modified R-script based on the version by V. Demichev was used to calculate MaxLFQ values (Github page, cit MaxLFQ). Data input was filtered for unique peptides, q-Value <0.01, Lib.Q.Value < 0.01, PG.Q.Value < 0.01, Global.Q.Value < 0.01, Quantity.Quality >0.7, Fragment.count≥4. MaxLFQ values were statistically analyzed with Perseus (V.1.6.5.0) [78]. Significance of differences was calculated with Students t-test with permutation-based false discovery rate (FDR) correction (FDR = 0.01). Venn diagrams were generated using the online tool from Bioinformatics & Evolutionary Genomics, University of Gent (https://bioinformatics.psb.ugent.be/webtools/Venn/). Results were visualized with Instant clue (V 0.11.3) [79].

4.12. Alcian blue staining

To stain deposited glycosaminoglycans, cells were washed with PBS and fixed with ice-cold methanol (Diagonal Münster) for 5 min. After repeated washing with PBS and with distilled water, cells were stained with Alcian blue (1 % Alcian blue, Merck KGaA/Sigma-Aldrich; in 0.5 M acidic acid, pH 2.5) for 3 h at room temperature. Remaining staining solution was removed with deionized water. Images were acquired with a bright field microscope, transformed into 8-bit grey scale images to assess the distribution of color over the entire image and presented in histograms using Fiji/ImageJ.

4.13. Statistical analysis

Statistical analysis of all results besides RNA-seq and mass spectrometry was performed using GraphPad Prism (GraphPad Software LLC). Appropriate tests for statistical significance are specified in the

figure legends.

CRediT authorship contribution statement

Isabel Zeinert: Writing – review & editing, Writing – original draft, Visualization, Validation, Methodology, Investigation, Formal analysis, Data curation. **Luisa Schmidt:** Writing – review & editing, Validation, Methodology, Formal analysis, Data curation. **Till Baar:** Writing – review & editing, Validation, Formal analysis. **Giulio Gatto:** Investigation, Methodology. **Anna De Giuseppe:** Writing – review & editing, Formal analysis. **Adelheid Korb-Pap:** Writing – review & editing, Resources, Funding acquisition, Conceptualization. **Thomas Pap:** Writing – review & editing, Resources, Funding acquisition, Conceptualization. **Esther Mahabir:** Writing – review & editing, Validation, Methodology, Formal analysis. **Frank Zaucke:** Conceptualization, Resources, Writing – review & editing. **Bent Brachvogel:** Writing – review & editing, Supervision, Conceptualization. **Marcus Krüger:** Writing – review & editing, Software, Resources, Methodology. **Thomas Krieg:** Writing – review & editing, Writing – original draft, Supervision, Resources, Formal analysis, Data curation, Conceptualization. **Beate Eckes:** Writing – review & editing, Writing – original draft, Supervision, Resources, Project administration, Funding acquisition, Formal analysis, Data curation, Conceptualization.

Funding

This study was supported by the German Research Foundation through FOR 2722 (ID 407239409 to BE, ID 407168728 to FZ, ID 384170921 to AKP and TP, and ID 384170921 to BB) and by the European Community's Horizon-MSCA-DN-01-01 under grant agreement n. 101072766 (CHANGE, GG and FZ).

Declaration of competing interest

The authors declare that they have no known competing financial interests or personal relationships that could have appeared to influence the work reported in this paper.

Acknowledgments

We thank all members of FOR 2722, in particular Julia Etich (Cologne) for stimulating discussion and sustained support. We acknowledge Sarah Göbbels (Cologne) for excellent assistance with cytokine assays and the Cologne Center for Genomics for help with the transcriptomics analysis. We furthermore thank the Regional Computing Center of the University of Cologne (RRZK) for providing computing time on the DFG-funded (Funding number: INST 216/512/1FUGG) High Performance Computing (HPC) system CHEOPS as well as support.

Appendix A. Supplementary data

Supplementary data to this article can be found online at https://doi.org/10.1016/j.yexcr.2025.114408.

Data availability

Data will be made available on request.

References

[1] A. Deichsel, et al., Collagen-binding integrin α11β1 contributes to joint destruction in arthritic hTNFtg mice, bioRxiv (2022) 2022, 01. 14.476301.
[2] R. Lafyatis, et al., Anchorage-independent growth of synoviocytes from arthritic and normal joints. Stimulation by exogenous platelet-derived growth factor and inhibition by transforming growth factor-beta and retinoids, J. Clin. Invest. 83 (4) (1989) 1267–1276.
[3] A. Korb, H. Pavenstadt, T. Pap, Cell death in rheumatoid arthritis, Apoptosis 14 (4) (2009) 447–454.
[4] G. Nygaard, G.S. Firestein, Restoring synovial homeostasis in rheumatoid arthritis by targeting fibroblast-like synoviocytes, Nat. Rev. Rheumatol. 16 (6) (2020) 316–333.
[5] R. Pelaez, et al., Integrins: moonlighting proteins in invadosome formation, Cancers 11 (5) (2019).
[6] A. Lauzier, et al., Formation of invadopodia-like structures by synovial cells promotes cartilage breakdown in collagen-induced arthritis: involvement of the protein tyrosine kinase Src, Arthritis Rheum. 63 (6) (2011) 1591–1602.
[7] J. Lehmann, et al., Grafting of fibroblasts isolated from the synovial membrane of rheumatoid arthritis (RA) patients induces chronic arthritis in SCID mice-A novel model for studying the arthritogenic role of RA fibroblasts in vivo, J. Autoimmun. 15 (3) (2000) 301–313.
[8] S. Lefevre, et al., Synovial fibroblasts spread rheumatoid arthritis to unaffected joints, Nat Med 15 (12) (2009) 1414–1420.
[9] J. Keffer, et al., Transgenic mice expressing human tumour necrosis factor: a predictive genetic model of arthritis, EMBO J. 10 (13) (1991) 4025–4031.
[10] A. Korb-Pap, et al., Early structural changes in cartilage and bone are required for the attachment and invasion of inflamed synovial tissue during destructive inflammatory arthritis, Ann. Rheum. Dis. 71 (6) (2012) 1004–1011.
[11] T. Pap, A. Korb-Pap, Cartilage damage in osteoarthritis and rheumatoid arthritis–two unequal siblings, Nat. Rev. Rheumatol. 11 (10) (2015) 606–615.
[12] C. Zeltz, D. Gullberg, α11β1: a mesenchymal collagen-binding integrin with a central role in tissue and tumor fibrosis, in: Integrins in Health and Disease: Key Effectors of Cell-Matrix and Cell-Cell Interactions, Springer, 2023, pp. 235–254.
[13] T. Pap, B. Eckes, A. Korb-Pap, Integrins in pathological tissue remodelling of joints, in: D. Gullberg, J.A. Eble (Eds.), Integrins in Health and Disease: Key Effectors of Cell-Matrix and Cell-Cell Interactions, Springer International Publishing, Cham, 2023, pp. 255–272.
[14] J.N. Schulz, et al., Reduced granulation tissue and wound strength in the absence of alpha11beta1 integrin, J. Invest. Dermatol. 135 (5) (2015) 1435–1444.
[15] C. Zeltz, et al., alpha11beta1 integrin is induced in a subset of cancer-associated fibroblasts in desmoplastic tumor stroma and mediates in vitro cell migration, Cancers 11 (6) (2019).
[16] S.N. Popova, et al., Alpha11 beta1 integrin-dependent regulation of periodontal ligament function in the erupting mouse incisor, Mol. Cell Biol. 27 (12) (2007) 4306–4316.
[17] S.R. Lamande, et al., Modeling human skeletal development using human pluripotent stem cells, Proc Natl Acad Sci U S A 120 (19) (2023) e2211510120.
[18] G.D. Jay, K.A. Waller, The biology of lubricin: near frictionless joint motion, Matrix Biol. 39 (2014) 17–24.
[19] B.C. Bernardo, et al., Cartilage intermediate layer protein 2 (CILP-2) is expressed in articular and meniscal cartilage and down-regulated in experimental osteoarthritis, J. Biol. Chem. 286 (43) (2011) 37758–37767.
[20] K. Bubb, et al., Mitochondrial respiratory chain function promotes extracellular matrix integrity in cartilage, J. Biol. Chem. 297 (4) (2021) 101224.
[21] N. Kondo, T. Kuroda, D. Kobayashi, Cytokine networks in the pathogenesis of rheumatoid arthritis, Int. J. Mol. Sci. 22 (20) (2021).
[22] A. Naba, et al., The matrisome: in silico definition and in vivo characterization by proteomics of normal and tumor extracellular matrices, Mol. Cell. Proteomics 11 (4) (2012). M111 014647.
[23] C. Wang, et al., Safflower yellow alleviates osteoarthritis and prevents inflammation by inhibiting PGE2 release and regulating NF-kappaB/SIRT1/AMPK signaling pathways, Phytomedicine 78 (2020) 153305.
[24] Y. Okada, Chapter 8 - proteinases and matrix degradation, in: G.S. Firestein, et al. (Eds.), Kelley and Firestein's Textbook of Rheumatology, tenth ed., Elsevier, 2017, pp. 106–125.
[25] C.F. Cheng, H.J. Liao, C.S. Wu, Tissue microenvironment dictates inflammation and disease activity in rheumatoid arthritis, J. Formos. Med. Assoc. 121 (6) (2022) 1027–1033.
[26] S. Hirakawa, et al., Marked induction of matrix metalloproteinase-10 by respiratory syncytial virus infection in human nasal epithelial cells, J. Med. Virol. 85 (12) (2013) 2141–2150.
[27] O.Y. Hong, et al., Inhibition of cell invasion and migration by targeting matrix metalloproteinase-9 expression via sirtuin 6 silencing in human breast cancer cells, Sci. Rep. 12 (1) (2022) 12125.
[28] P. Lu, et al., Extracellular matrix degradation and remodeling in development and disease, Cold Spring Harb Perspect Biol 3 (12) (2011).
[29] S. Ricard-Blum, R. Salza, Matricryptins and matrikines: biologically active fragments of the extracellular matrix, Exp. Dermatol. 23 (7) (2014) 457–463.
[30] A.M. Haack, C.M. Overall, U. Auf dem Keller, Degradomics technologies in matrisome exploration, Matrix Biol. 114 (2022) 1–17.
[31] X. Wang, et al., Overexpression of human matrix metalloproteinase-12 enhances the development of inflammatory arthritis in transgenic rabbits, Am. J. Pathol. 165 (4) (2004) 1375–1383.
[32] B. Fingleton, Matrix metalloproteinases as regulators of inflammatory processes, Biochim. Biophys. Acta Mol. Cell Res. 1864 (11 Pt A) (2017) 2036–2042.
[33] S. Hey, S. Linder, Matrix metalloproteinases at a glance, J. Cell Sci. 137 (2) (2024).
[34] M.A. Murayama, et al., Chemokines and chemokine receptors as promising targets in rheumatoid arthritis, Front. Immunol. 14 (2023) 1100869.
[35] A. Schulte, et al., Sequential processing of the transmembrane chemokines CX3CL1 and CXCL16 by alpha- and gamma-secretases, Biochem. Biophys. Res. Commun. 358 (1) (2007) 233–240.
[36] M. Tohyama, et al., CXCL16 is a novel mediator of the innate immunity of epidermal keratinocytes, Int. Immunol. 19 (9) (2007) 1095–1102.

[37] J.J. Haringman, et al., Chemokine and chemokine receptor expression in paired peripheral blood mononuclear cells and synovial tissue of patients with rheumatoid arthritis, osteoarthritis, and reactive arthritis, Ann. Rheum. Dis. 65 (3) (2006) 294–300.
[38] M. Liu, et al., Association of increased expression of macrophage elastase (matrix metalloproteinase 12) with rheumatoid arthritis, Arthritis Rheum. 50 (10) (2004) 3112–3117.
[39] L. Zhang, et al., Accumulation of nicotinamide N-methyltransferase (NNMT) in cancer-associated fibroblasts: a potential prognostic and predictive biomarker for gastric carcinoma, J. Histochem. Cytochem. 69 (3) (2021) 165–176.
[40] M.A. Eckert, et al., Proteomics reveals NNMT as a master metabolic regulator of cancer-associated fibroblasts, Nature 569 (7758) (2019) 723–728.
[41] T. Pap, et al., Synovial fibroblasts and articular tissue remodelling: role and mechanisms, Semin. Cell Dev. Biol. 101 (2020) 140–145.
[42] M. Aumailley, The laminin family, Cell Adh Migr 7 (1) (2013) 48–55.
[43] J.G. Pickering, et al., Coordinated effects of fibroblast growth factor-2 on expression of fibrillar collagens, matrix metalloproteinases, and tissue inhibitors of matrix metalloproteinases by human vascular smooth muscle cells. Evidence for repressed collagen production and activated degradative capacity, Arterioscler. Thromb. Vasc. Biol. 17 (3) (1997) 475–482.
[44] B.M. Steiglitz, D.R. Keene, D.S. Greenspan, PCOLCE2 encodes a functional procollagen C-proteinase enhancer (PCPE2) that is a collagen-binding protein differing in distribution of expression and post-translational modification from the previously described PCPE1, J. Biol. Chem. 277 (51) (2002) 49820–49830.
[45] J. Wang, et al., A new subtype of multiple synostoses syndrome is caused by a mutation in GDF6 that decreases its sensitivity to noggin and enhances its potency as a BMP signal, J. Bone Miner. Res. 31 (4) (2016) 882–889.
[46] R.E. Kuestner, et al., Identification of the IL-17 receptor related molecule IL-17RC as the receptor for IL-17F, J. Immunol. 179 (8) (2007) 5462–5473.
[47] Y. Hu, et al., The IL-17 pathway as a major therapeutic target in autoimmune diseases, Ann. N. Y. Acad. Sci. 1217 (2011) 60–76.
[48] K. Shimizu, et al., IL-1 receptor type 2 suppresses collagen-induced arthritis by inhibiting IL-1 signal on macrophages, J. Immunol. 194 (7) (2015) 3156–3168.
[49] K. Wei, H.N. Nguyen, M.B. Brenner, Fibroblast pathology in inflammatory diseases, J. Clin. Invest. 131 (20) (2021).
[50] S.R. Pickens, et al., Characterization of CCL19 and CCL21 in rheumatoid arthritis, Arthritis Rheum. 63 (4) (2011) 914–922.
[51] Y. Yan, et al., CCL19 and CCR7 expression, signaling pathways, and adjuvant functions in viral infection and prevention, Front. Cell Dev. Biol. 7 (2019) 212.
[52] K. Wakabayashi, et al., Eotaxin-1/CCL11 is involved in cell migration in rheumatoid arthritis, Sci. Rep. 11 (1) (2021) 7937.
[53] R Core Team, R: a language and environment for statistical computing, Available from: https://www.R-project.org/, 2023.
[54] Posit Team, RStudio: integrated development environment for R [cited 2023 18.07.2023]; Available from: http://www.posit.co/, , 2023.
[55] M. Martin, Cutadapt removes adapter sequences from high-throughput sequencing reads, EMBnet. journal 17 (1) (2011) 10–12.
[56] A. Dobin, et al., STAR: ultrafast universal RNA-seq aligner, Bioinformatics 29 (1) (2013) 15–21.
[57] Y. Liao, G.K. Smyth, W. Shi, featureCounts: an efficient general purpose program for assigning sequence reads to genomic features, Bioinformatics 30 (7) (2014) 923–930.
[58] Y. Liao, G.K. Smyth, W. Shi, The Subread aligner: fast, accurate and scalable read mapping by seed-and-vote, Nucleic Acids Res. 41 (10) (2013) e108.
[59] H. Wickham, ggplot2: Elegant Graphics for Data Analysis, Springer-Verlag, New York, 2016.
[60] T. Van den Brand, Hacks for 'ggplot2 (2023) ggh4x [cited 2023 18.07.2023]; Available from: https://CRAN.R-project.org/package=ggh4x.
[61] K. Slowikowski, Ggrepel: automatically position non-overlapping text labels with 'ggplot2' [cited 2023 18.07.2023]; Available from: https://CRAN.R-project.org/package=ggrepel, 2023.
[62] Z. Gu, et al., Circlize Implements and enhances circular visualization in R, Bioinformatics 30 (19) (2014) 2811–2812.
[63] H. Wickham, Stringr: simple, consistent wrappers for common string operations [cited 2023 18.07.2023]; Available from: https://CRAN.R-project.org/package=stringr, 2022.
[64] H. Wickham, et al., Dplyr: a grammar of data manipulation [cited 2023 18.07.2023]; Available from: https://CRAN.R-project.org/package=dplyr, 2023.
[65] M.I. Love, W. Huber, S. Anders, Moderated estimation of fold change and dispersion for RNA-seq data with DESeq2, Genome Biol. 15 (12) (2014) 550.
[66] M. Carlson, org.Mm.eg.db: genome wide annotation for Mouse [cited 2023 18.07.2023]; Available from: https://www.bioconductor.org/packages//2.7/data/annotation/html/org.Mm.eg.db.html, 2022.
[67] J. Melville, Uwot: the Uniform Manifold Approximation and Projection (UMAP) Method for Dimensionality Reduction, 2022.
[68] V. Todorov, P. Filzmoser, An object-oriented framework for robust multivariate analysis, J. Stat. Software 32 (3) (2009) 1–47.
[69] Z. Gu, Complex heatmap visualization, Imeta 1 (3) (2022) e43.
[70] Z. Gu, R. Eils, M. Schlesner, Complex heatmaps reveal patterns and correlations in multidimensional genomic data, Bioinformatics 32 (18) (2016) 2847–2849.
[71] T. Wu, et al., clusterProfiler 4.0: a universal enrichment tool for interpreting omics data, Innovation 2 (3) (2021) 100141.
[72] H. Wickham, et al., Svglite: an 'SVG' graphics device [cited 2023 18.07.2023]; Available from: https://CRAN.R-project.org/package=svglite, 2023.
[73] L. McInnes, J. Healy, J. Melville, Umap: Uniform manifold approximation and projection for dimension reduction, arXiv (2018) arXiv:1802.03426.
[74] L. Spitznagel, et al., Characterization of a pseudoachondroplasia-associated mutation (His587–>Arg) in the C-terminal, collagen-binding domain of cartilage oligomeric matrix protein (COMP), Biochem. J. 377 (Pt 2) (2004) 479–487.
[75] C.S. Hughes, et al., Single-pot, solid-phase-enhanced sample preparation for proteomics experiments, Nat. Protoc. 14 (1) (2019) 68–85.
[76] Y. Perez-Riverol, et al., The PRIDE database resources in 2022: a hub for mass spectrometry-based proteomics evidences, Nucleic Acids Res. 50 (D1) (2022) D543–D552.
[77] V. Demichev, et al., DIA-NN: neural networks and interference correction enable deep proteome coverage in high throughput, Nat. Methods 17 (1) (2020) 41–44.
[78] S. Tyanova, T. Temu, J. Cox, The MaxQuant computational platform for mass spectrometry-based shotgun proteomics, Nat. Protoc. 11 (12) (2016) 2301–2319.
[79] H. Nolte, et al., Instant clue: a software suite for interactive data visualization and analysis, Sci. Rep. 8 (1) (2018) 12648.